Tribological and corrosion performance of electrodeposited Ni–Fe/Al$_2$O$_3$ coating

Mohammad Rezayat [a,b,*], Morteza Saghafi Yazdi [a], Mohammad Damous Zandi [c], Aref Azami [c]

[a] *Department of Materials Science and Engineering, Faculty of Engineering, Imam Khomeini International University, Qazvin, 34149, Iran*
[b] *CIEFMA-Department of Materials Science and Engineering, Universitat Politècnica de Catalunya-BarcelonaTECH, 08019, Barcelona, Spain*
[c] *Department of Mechanical Engineering, Universitat Politècnica de Catalunya-BarcelonaTECH, 08019, Barcelona, Spain*

ARTICLE INFO

ABSTRACT

Nickel–Iron coating was formed from a sulfate base electroplating bath under a current density of 3 A/dm^2 and turbulence of 300 rpm on a previously prepared cylindrical steel substrate. In order to obtain a sample including nickel composite coating, different amounts of alumina particle powder were added to the plating solution of the sample in question. By adding different quantities of ferrous sulfate to the electroplating bath under a current density of 2.5 A/dm^2 and turbulence of 300 rpm, an optimal sample containing 20 g/L of ferrous sulfate was obtained was free of any stress and microcracks. A hardness test was performed for the optimal sample among the nickel–iron composite samples, and the sample containing 50 g/L of alumina particles was selected as the optimal sample. The Ni–Fe/Al$_2$O$_3$ composite sample was tested for hardness, corrosion and wear. The obtained results showed that the highest hardness level is equivalent to 740 HV and the best corrosion resistance with the most positive corrosion potential. The lowest amount of wear mass is equal to 0.1 mg, and it showed the highest wear resistance.

1. Introduction

Nowadays, the demand in various industries for high-performance components is increasing rapidly. One of the most critical factors in growing parts' performance and service life is their surface quality (Azami et al., 2020). In various industries, the surfaces of industrial parts are constantly exposed to mechanical, thermal, chemical, and electrochemical forces and loads, which can cause surface and subsurface damage (Karmakar et al., 2020). The surface coating process is one technique that increases the performance and service life of parts by increasing the hardness, wear resistance, and corrosion resistance (Torabinejad et al., 2016; Wasekar and Sundararajan, 2015).

One of the coating techniques that has been developed in recent years is composite multilayer (ML) coating (Torabinejad et al., 2017d; Raghavendra et al., 2018). This method uses two or more alternative layers with different compositions and properties (Torabinejad et al., 2017c). Compared to the monolithic coating method, due to the high hardness of the layers and graded microstructures, the surface properties such as mechanical, electrochemical, optical, and oxidation resistance are significantly increased (Majidi and Aliofkhazraei, 2016; Srivastava et al., 2007; Fiebig others, 2016). Also, composite multilayer coatings not only have lower shear stress but also show a good ability to prevent crack growth, which increases the lifetime properties of

the part (Torabinejad, 2016; Gupta and Podlaha, 2010). Selecting the appropriate material and designing its layer thickness are effective factors in this method (Zhang et al., 2015). Multilayer coatings are divided into several categories, which are metal–ceramic multilayer (Maillé et al., 2004; Major, 2014), ceramic–ceramic multilayer (Kim et al., 2004; Troyon and Wang, 1996), alloy multilayer (Etminanfar and Heydarzadeh Sohi, 2012; Lajevardi et al., 2013), and multilayer Composite (Thiemig et al., 2009). various methods are used to produce multilayer coatings, such as chemical vapor deposition (CVD), physical vapor deposition (PVD), thermal plasma spray (TPS), and electrodeposition (Chandrasekar and Pushpavanam, 2008). However, because the electro-coating process has advantages such as low coating temperature, lower start-up, cost-effectiveness, and the ability to control the thickness of the layers, in recent decades, it has received more attention than other methods (Chaudhari and Singh, 2018). Also, in this method, the applied flow required for the layering process can be controlled through electronic devices and microprocessors (Asa Deepthi others, 2016). Electrodeposition, also known as electroplating, is a chemical process in which an electric current is applied to reduce metal cations in a solution. The surface layer is coated, and the surface structure is modified (Aliofkhazraei others, 2021). In this method, water is usually used as a solvent, and the required current for the process is established

by connecting two electrodes to an external power supply. By performing chemical reactions between the electrolyte and electrodes, ions are deposited from the electroplating bath onto the surface. In this method. The anode acts as the deposited material and the layer to be coated acts as the cathode. The main purpose of this process is uniform deposition to produce monolithic or multilayer coatings (Sajjadnejad et al., 2014; Torabinejad et al., 2017a). The current required for the electrodeposition process can be supplied as direct current (DC) or pulse current (PC). The direct electric current required for the process is continuously transmitted to the system in the pulse current method; the required electric current is rapidly changing between the two values (Torabinejad et al., 2017a). The advantages of electrodeposition are high coating rate, the possibility of producing composite coatings by combining different properties through changing the coating parameters, the ability to produce materials with micrometer–nanometer dimensions, low equipment cost, low working temperature, high purity, the possibility of coating on different substrates, and industrial applications (Góral et al., 2014; Chintada et al., 2021). Due to their high hardness, wear resistance, and corrosion resistance, nickel-based composite coatings such as Ni–Fe (Alimadadi et al., 2009), Ni–W (Vitry et al., 2012), Ni–P (Torabinejad et al., 2017b), Ni–Cu, Ni–Cr (Torabinejad et al., 2017b), and Ni–Al_2O_3 have been considered in recent years. The researchers also increased their tribological properties by adding hard ceramic particles to the second phase of nickel-based coatings. Also, some research has been done on adding micro/nanoparticles such as SiC (Ataee-Esfahani et al., 2009), Si3N4 (Starosta and Zielinski, 2004), Al_2O_3 (Alimadadi et al., 2009; Rezayat et al., 2020), and Sn–Cu nano antibacterial powder (Rezayat et al., 2020), the Ni–Fe matrix. Reports indicate that Ni–Fe–Al_2O_3 coating has good tribological properties. Starosta and Zielinski (2004) investigate the effects of Ni–Fe and Ni–Fe–Al_2O_3 multilayer coatings on corrosion and wear resistance of cast iron RVK (Daros). They found that increasing the amount of Fe and Al_2O_3 had a hurt increased the wear resistance by at least 20% compared to the Ni coating state. Torabinejad et al. (2017b) investigated the effects of the duty cycle-decreased method (DDM) and frequency-increased method (FIM) for Ni–Fe–Al_2O_3 multilayer nanocomposites for low carbon iron workpiece. They claimed that DDM compared to FIM, reduced the corrosion current density and wear rate by 50 and 20, respectively. Torabinejad et al. (2016) studied the effects of frequency and duty cycle on Ni–Fe–Al_2O_3 multilayer coating by intermittent electrodeposition method and its effect on wear and corrosion for low carbon iron workpiece. They found that although a change in frequency had not significantly affected the deposition of nanoparticles or the Ni and Fe content, a change in the duty cycle caused a change in their content. They also claimed that a constant change in frequency between 100 and 6400 Hz increased the corrosion resistance and wear of composite multilayer (ML) coatings. Torabinejad et al. (2017a) investigated the microstructural effects of monolithic and multilayer (ML) Ni–Fe–Al_2O_3 coatings on mechanical properties and wear resistance of low carbon steel (SAE-1008). They showed that using ML coatings improves mechanical properties, microstructures, and wear resistance compared to monolithic coatings. Torabinejad et al. (2017c) investigated the wear behavior behaviour effects of the multilayer (ML) structure of Ni–Fe–Al_2O_3 coatings of AISI 1008 steel. They found that reducing the thickness of the ML coating layers increased the hardness and wear resistance.

The literature review shows that the focus of previous research has been more on Ni–Fe–Al_2O_3 multilayer (ML) composite coatings. So far, little research has been done on the composition of Fe and Al_2O_3 (Fe/Al_2O_3) nanoparticles. Therefore, the different effects of the combination of Fe and Al_2O_3 nanoparticles must be further studied. This study aimed to investigate the impact of various amounts of other Fe and Al_2O_3 nanoparticles on the tribological behavior and corrosion of Ni composite coatings. This study studied the change in Fe and Al_2O_3 values and their effects on the mechanical properties of the st37 carbon steel workpiece. Wear and corrosion tests were used to evaluate the mechanical and tribological properties of Ni–Fe/Al_2O_3 coatings.

2. Materials and methods

2.1. Material

Carbon steels, especially low carbon steels, due to their high forging and machining capabilities, are widely used in various industries such as automotive, bridge construction, building construction, oil, and shipping industries (Torabinejad, 2016). In this study, the specimens were formed in two different shapes regarding experimentations made of St37 carbon steel [Table 1], the cylindrical shape with Ø10 mm diameters and 50 mm height for hardness, corrosion, X-ray diffraction (XRD), and Scanning electron microscopy (SEM), and the cubic shape with dimension $25 * 15 * 2$ mm for tribological properties. All the samples were abraded with sandpaper (360, 600, 800, and 1200 grits) to make a smooth surface; then degreasing was done ultrasonically for 1 min in ethanol. Finally, the samples were rinsed for 10 s in distilled water with 10 Wt% of hydrochloric acid solution. All the powders used in this study (Ni and Fe) had 93% purity and grain size of about 25 μm from Fluka company (Buchs, Switzerland).

2.2. Coating bath

Since the objective of this study is electrical plating, the nickel was used as an anodic part in a cubic shape of $50 * 25 * 10$ mm dimension in a bath containing 100 ml of electrolyte liquid.

Temperature, pH of the bath, current density, and stirring speed were 55 °C, 3.5, 3 A/dm^2, and 300 rpm, respectively. The pH was controlled by applying CHY 392R digital pH meter. The coating bath content [Table 2] included all elements used for the electroplating process.

Four different nanocomposite Ni–Fe/Al_2O_3 samples were achieved and considered by adding various alumina particles of 10 g/L, 30 g/L, 50 g/L, and 70 g/L to the initial container (with the same abovementioned contents) sequentially.

St37 steel (DIN 17100) was connected to the negative pole of the DC rectifier, and the positive pole was the nickel anode. After applying the electrical current, the electrodeposition coating process was started by hydrogen restoring and hydrolysis reactions in the solution. All samples were exposed to the same condition for 1 h and 45 min. The bath and plating conditions were the same for all models, but the amounts of alumina added to the plating bath were different.

The cross-sectional and metallography methods according to ASTM-B487 standard at 200X magnification were used to calculate the thickness of the coating layer (150 μm) [Fig. 1].

2.3. Characterization methods

2.3.1. X-ray diffraction (XRD)

Crystal structure, the composition of phases, preferred orientation and grain size were determined by X-ray diffraction model D8 DIS-COVER from Bruker and in this X-ray device, Cu–Kα radiation with $\lambda = 1.5406$ Å wavelength, created under a potential difference of 40 keV, a current intensity of 40 mA and a scanning speed of 0.015°/s was used. Also, the obtained patterns were characterized by MAUD (this is Free software and is NOT under any license), and the angular step was calculated.

2.3.2. Scanning electron Microscopy (SEM)

The morphology of the coatings was investigated by the MIRA3 scanning electron microscope made by TESCAN company with the resolution of 1.5 nm at 15 kV and 4.5 nm at 1 kV. A resolution of 15 kV was used for imaging, and the distance of the electron beam from the sample was 4.9 mm. Backscatter electrons characterized the images of alloy and composite coatings by secondary electrons.

Table 1
Mechanical properties and chemical compositions of St 37 carbon steel.

Mechanical properties			Chemical compositions				
Yield stress (MPa)	Ultimate tensile strength (MPa)	Elongation (%)	C (%)	Mn (%)	P (%)	S (%)	Cu (%)
315	372	36	0.190	1.500	0.045	0.045	0.600

Table 2
The main contents and quantities of the coating bath.

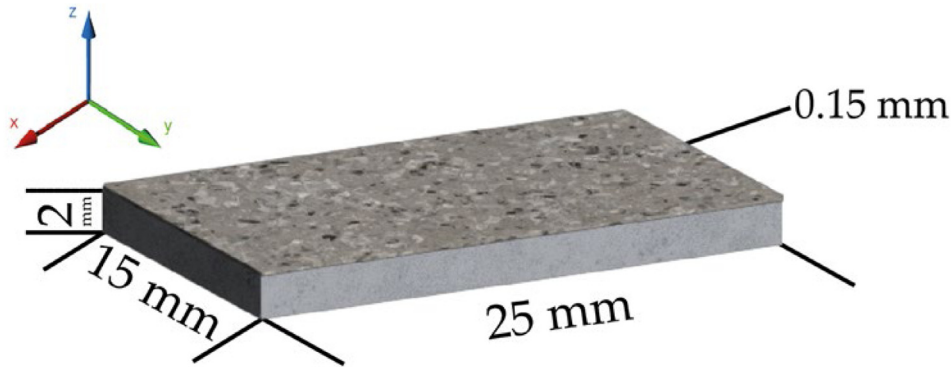| Content	Sodium dodecyl sulfate (SDS)	Boric acid	Nickel chloride	Nickel sulfate	Saccharin	Iron sulfate	Sodium citrate
Quantity	0.1 g/L	35 g/L	45 g/L	250 g/L	3 g/L	20 g/L	25 g/L

Fig. 1. Schematic of the sample with accurate dimensions (upper layer is the coating layer).

2.4. Hardness test

Microhardness was obtained by the Struers model Durmin and IVIUM Vertex hardness tester. The applied load time was 10 s and applied to the amount of 490.3 mN (HV 0.05). Five hardness points were taken from each sample, and their average was considered microhardness.

2.5. Corrosion resistance test by the potentiostat

The corrosion resistance test for the coatings created in this research was investigated according to ASTM G102-89, G59-97, G1-03, G3-89, and G5-94 standards using potentiostat equipment.

IVIUM Vertex potentiostat device was used to measure the corrosion resistance of the samples. For this purpose, the saturated calomel electrode was used as the reference electrode, the platinum electrode was used as the counter electrode, and the coated samples were used as the working electrode. It was done for the samples so that the tested surface was the same for all the samples.

In the investigations, first, the samples were placed in a 3% sodium chloride solution for 30 min to obtain the equilibrium potential (EOCP) and stabilize it. Then, I–V curves were obtained with a scanning speed of 1 mV/s and a scanning range of $\pm$10 mV relative to the equilibrium potential to calculate the coating resistance at room temperature. In the following, Tafel curves are drawn with a scanning speed of 1 millivolt-second and a scanning range of $\pm$300 mV relative to the equilibrium potential at room temperature.

First, to obtain the equilibrium potential (EOCP), the samples were placed in sodium chloride solution (3%) for 30 s. Then, the I–V curves were measured with a scanning speed of 1 mV/s and a scanning range of $\pm$10 mV relative to the equilibrium potential to calculate the coating resistance at room temperature. In the following, Tafel curves were obtained with a scanning speed of 1 millivolt per second and a scanning range of $\pm$300 mV relative to the equilibrium potential at room temperature.

2.6. Abrasion resistance test

A 100Cr6 steel pin (DIN 1.2067) with a diameter of 5 mm, a front curvature of 5 mm, and a hardness of 825 $\pm$ 15 HV10 was used on the disk at room temperature (25 °C) to measure the wear resistance of the coatings.

The force applied to perform the wear test was 6 newtons, the distance covered was 100 m in a circle with a radius of 5 mm, the rotation speed was 95 rpm, and the rate was 0.05 m/s. The mass reduction friction coefficient was obtained by considering the above conditions. In order to increase the accuracy of weighing the samples before and after the wear test, the samples were placed in ethanol solution and subjected to ultrasound waves in an ultrasonic device for one hour to remove contamination and wear products.

3. Results and discussions

3.1. X-ray diffraction (XRD)

Fig. 2 shows the X-ray diffraction patterns of pure nickel coatings. As shown in Fig. 1, the peaks on planes (220), (200), and (111) all indicate pure nickel and the FCC crystal structure. The preferred crystal growth in these planes is indicated by the peak intensities of planes (200) and (111).

As can be seen in Fig. 2, because of having the highest intensity, the crystal plane (200) is the principal plane of the coating growth, known as one of the characteristics of direct current electrical deposition.

By adding the alumina particles to the sediment structure, it was observed that the peak of planes (200) and (111) still showed the preferred crystal growth of nickel in these planes. However, the peak of the plate (200) was reduced, and the plane growth preference changed to (111). New peaks mean new phases in the XRD diagram, 35°, 58°, and shift peaks show Hercinite ($FeAl_2O_4$), Hematite(Fe_2O_3), and some Aluminum Iron Oxide ($AlFeO_3$) (Al-Faysal, 2018).
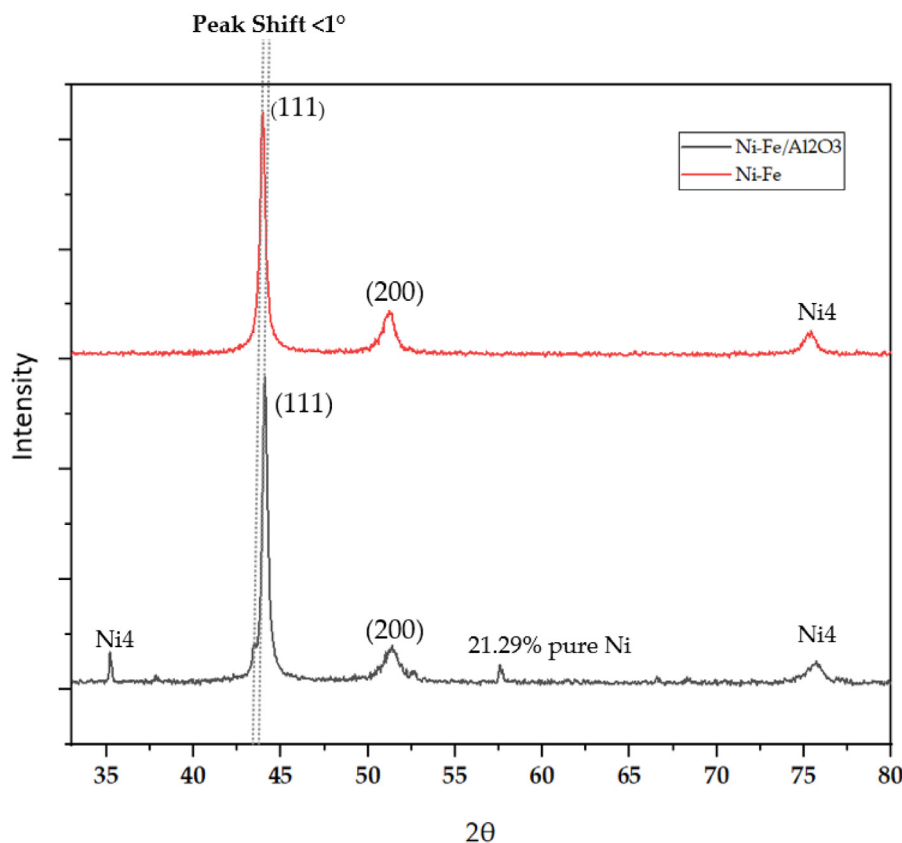
Fig. 2. XRD pattern of Ni–Fe/Al$_2$O$_3$ and new phases and crystallographic planes.

3.2. Micro-hardness

As shown in Fig. 3, the hardness was increased by increasing the amount of alumina added to the solution due to the greater placement of these particles in the coating.

Alumina particles, due to their high hardness (ceramic structural), increase the hardness of the coating. On the other hand, they have also avoided dislocation movements, according to the Hall–Petch relationship (Lumley et al., 2006). The hardness increases by activating scattering hardness mechanisms that limit the movement of dislocations and grain boundaries of the coating.

According to Fig. 3, the sample containing 50 g/L aluminas had the highest hardness among the samples. This hardness was due to a complex background and a volume fraction of alumina particles in the coating (Bonino, 1997).

3.3. Scanning Electron Microscopy (SEM), Energy Dispersive X-ray spectroscopy (EDX)

Fig. 4 shows the morphology of Ni–Fe/Al$_2$O$_3$ composite alloy coatings with different amounts of alumina particles. The Ni–Fe/Al2O3 alloy coating is spherical and uniform based on these morphological forms. By placing alumina particles as a reinforcement in the composite alloy coating, the spherical structure of the layer becomes more delicate and relatively flat (Torabinejad, 2016), which can be due to changes in the growth mechanism.

Micro-Hardness of composite alloy coatings and the direct effect of this parameter on the required abrasion resistance and also the optimal distribution of alumina particles in the layer are shown in Figs. 4 and 5 related to the map of the elements in the composition area, the combined coating of electrolyte containing 70 g/l of alumina particles was considered the optimal state of Ni–Fe/current alloy composite coatings for future tests and studies.

Table 3
Electrochemical results from the polarization curves of Ni and Ni–Fe/Al$_2$O$_3$ coatings.

Coat type	i_{Corr} (A/cm^2)	E_{Corr} (mV)
Ni	1.2	−504
Ni–Fe/Al$_2$O$_3$	1.8	−336

3.4. The corrosion resistance of Ni and Ni–Fe/Al$_2$O$_3$ composite coating

The result of the corrosion resistance test for the Ni–Fe/Al$_2$O$_3$ composite sample with 50 g/L alumina powder in the electrolyte, which was considered the optimal sample, is shown in Fig. 6.

Table 3 shows the electrochemical results from the polarization curves of the Ni–Fe/Al$_2$O$_3$ composite sample compared to the Ni sample that is associated with increased corrosion potential and decreased corrosion current density, which indicates an increase in corrosion resistance for the combined sample.

The results were obtained from the average of 10 polarization curves. The corrosion current density for the samples was also calculated from the Stern–Geary equation.

Varna quest diagrams help to show Ni coatings and Ni–Fe/Al$_2$O$_3$ composite coatings [Fig. 7] and corrosion resistance of composite coatings in the form of composition alloy.

Since alumina hardeners are a ceramic phase, there is a very high corrosion resistance on the coating surface between the corrosive solution and the coating, which causes corrosion on the metal base at the grain boundary. Covering these centers, which have high energy, the areas are prone to corrosion. Lumley et al. (2006) reported that maximum hardness exists when there is 30% of Al$_2$O$_3$ in the coat. Also, according to their ANOVA examination, it is clear that the amount of Al$_2$O$_3$ is predominant in affecting the hardness, while current density has a relatively low impact.
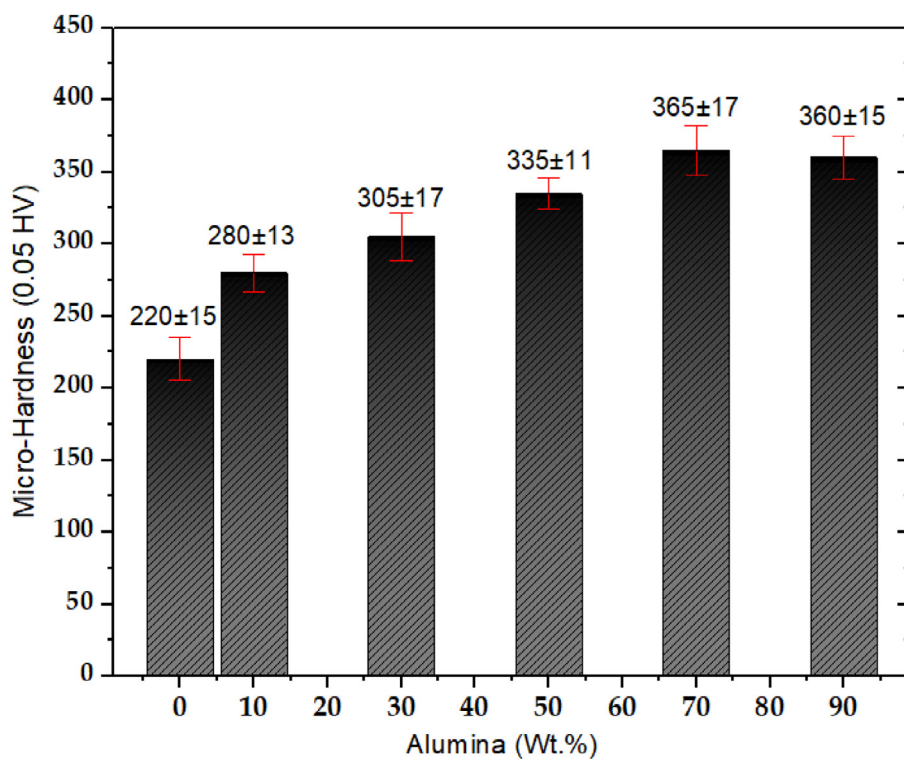
Fig. 3. Effect of the presence of alumina particles on the micro-hardness of Ni–Fe/Al$_2$O$_3$ alloy-composite coating.
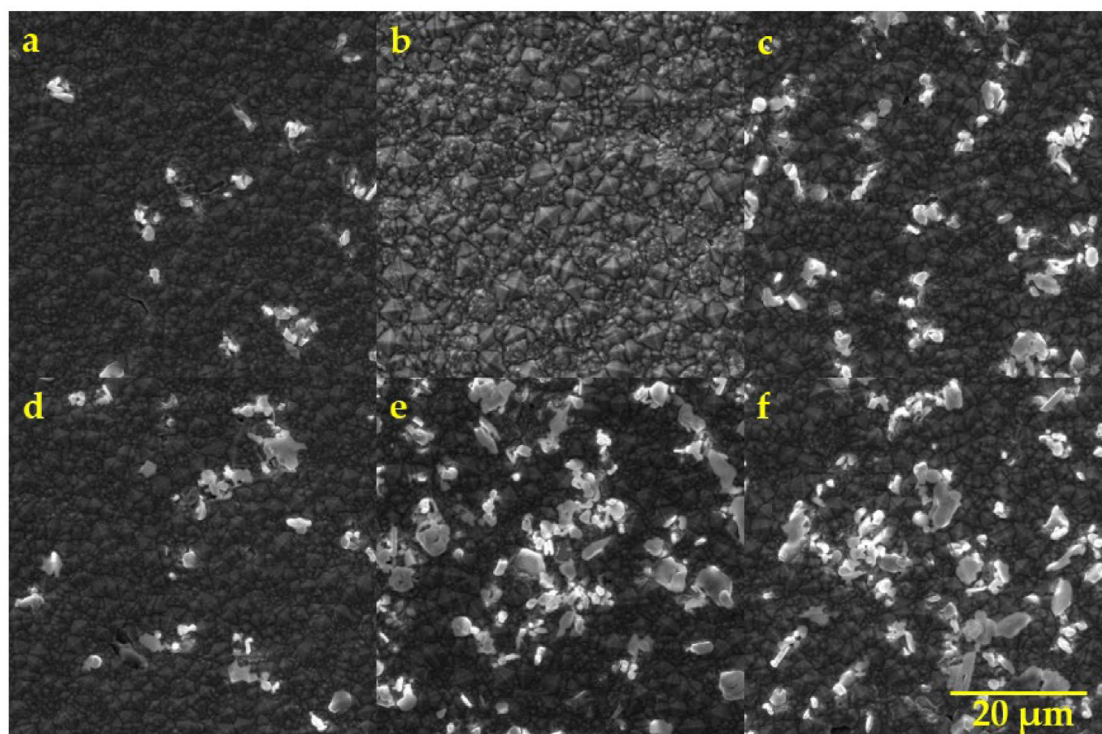

Fig. 4. SEM images of Ni–Fe/Al$_2$O$_3$ alloy coating morphology (a) 0 g/l alumina, (b) 10 g/l alumina, (c) 30 g/l alumina, (d) 50 g/l alumina, (e) 70 g/l alumina, (f) 90 g/l alumina.

3.5. Wear resistance

According to the results in Table 4 and the amount of mass reduction in the wear band, the wear resistance was increased for Ni, and Ni–Fe/Al$_2$O$_3$ coatings, respectively.

Fig. 8 shows the changes related to the coatings of Ni and Ni–Fe/Al$_2$O$_3$. Since the hardness of the Ni–Fe/Al$_2$O$_3$ sample is higher than that of the Ni sample, the wear bar width and wear rate were reduced. The presence of alumina hardening particles and increasing the hardness increase the wear resistance and changes the wear mechanism from layered wear to scratch abrasion. Lumley et al. (2006) noted
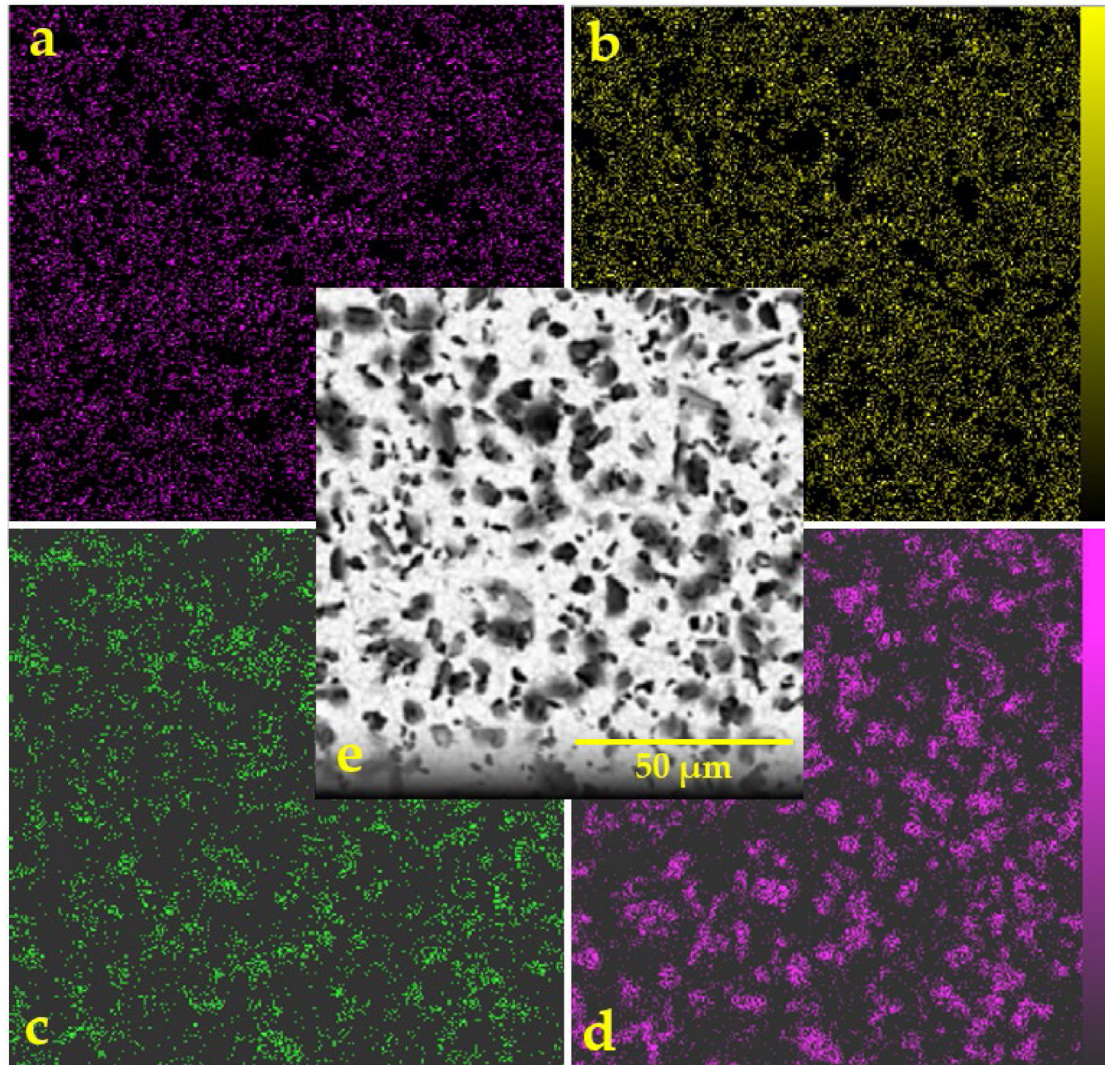
Fig. 5. Distribution of elements in Ni–Fe/Al$_2$O$_3$ composite alloy coatings (a) Iron, (b) Nickel, (c) Oxygen, (d) Aluminum.

Table 4
The wear resistance information for Ni and Ni–Fe/Al$_2$O$_3$ coatings.

Wear	Friction coefficient (μ)	Width of wear bar (mm)	Mass of the wear bar (mg)
Ni	0.23	0.8–1.27	0.7
Ni–Fe/Al$_2$O$_3$	0.35	0.56	0.1

significant differences in the friction coefficient of the pure Ni and Ni–Fe/Al$_2$O$_3$ composite. These differences were attributed to the changes in the microstructure of the matrix caused by the embedded Al$_2$O$_3$ particles.

Fig. 8 shows the friction coefficient variations for Ni coatings and Ni–Fe/Al$_2$O$_3$ composite coatings. The coefficient of friction of Ni coating is lower than that of Ni–Fe/Al$_2$O$_3$ composite coating, which can be related to the change in wear mechanism from layer wear mechanism to scratch wear mechanism. The coefficient of friction for the coating of Ni is unstable, which indicates the repeated loss of the tribological layer.

Adding the alumina particles to the coating increased the intensity of this crystal plane (111); the high density of this crystal plane can also be considered a factor in reducing the wear rate in Ni–Fe/Al$_2$O$_3$ composite coating.

Fig. 9 shows the wear bar SEM image and morphology of the Ni–Fe/Al$_2$O$_3$ composite coating. As the hardness of the Ni–Fe/Al$_2$O$_3$ sample is higher than the Ni sample, the width of the wear bar and the wear rate are reduced. The presence of alumina hardening particles and increasing the hardness increase the wear resistance and changes the wear mechanism from layered wear to scratch abrasion.

4. Conclusion

In this study, the effects of different amounts of different combinations of Fe and Al$_2$O$_3$ nanoparticles on the tribological behavior and corrosion of Ni composite coatings were investigated. For this purpose, the change in Fe and Al$_2$O$_3$ values and their effects on the mechanical properties of the St37 carbon steel workpiece were studied. According to the experiments performed on the composite coating, the following results were obtained:

1. XRD diagrams confirmed the existence of new phases in the sample. The new peaks in the diagrams are related to the new phase that has been created since the addition of alumina particles to the coating so that planes (111) and (200) continue to grow because the ceramic grains of Al$_2$O$_3$ are placed on a strict background such as nickel, which in this case has more mechanical properties and also causes three new phases of Hercinite (FeAl$_2$O$_4$), Hematite (Fe$_2$O$_3$), and some Aluminum Iron Oxide (AlFeO$_3$).
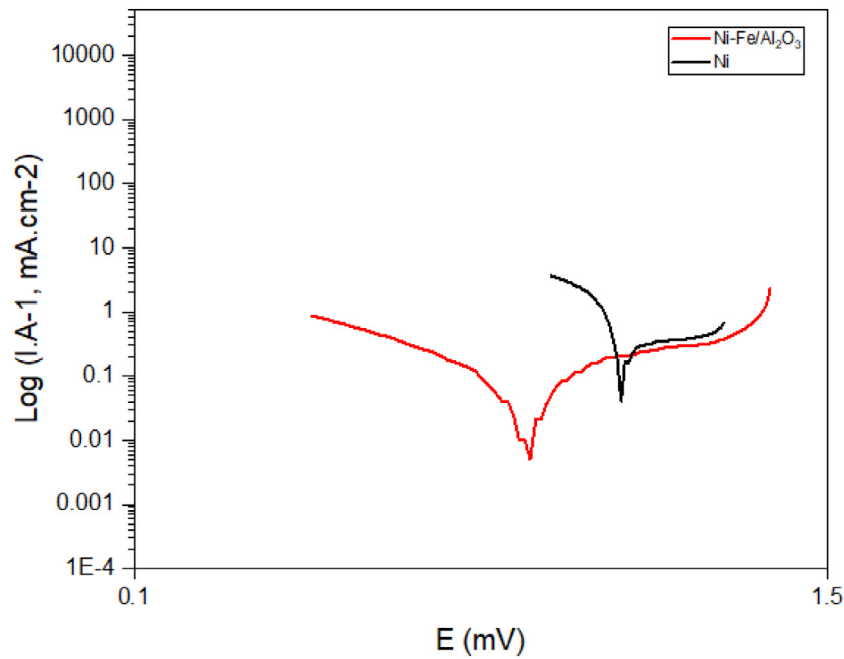
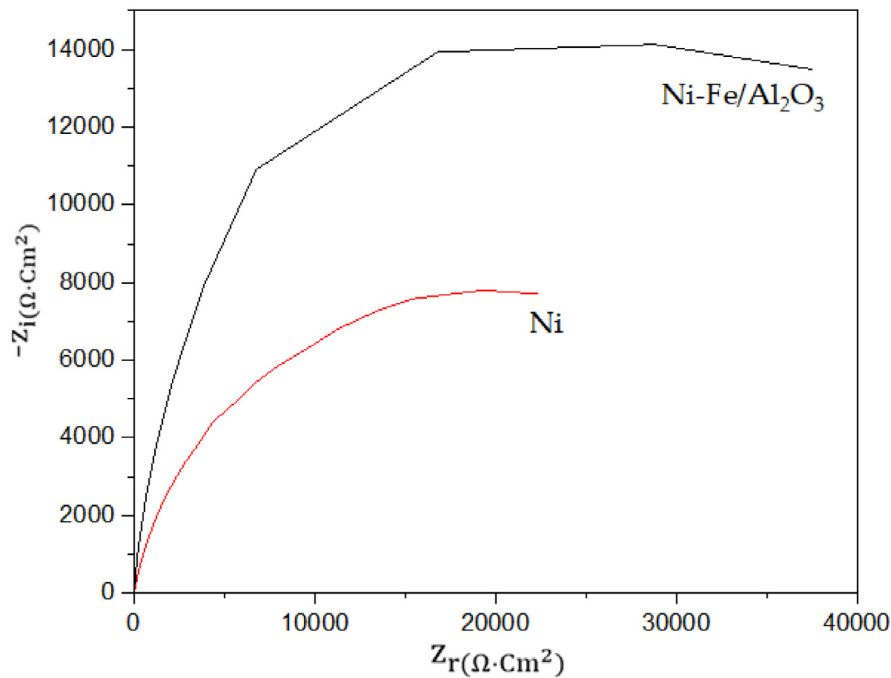**Fig. 6.** Polarization diagram for Ni and Ni–Fe/Al_2O_3 coatings.

Fig. 7. Varna quest diagram of Ni and Ni–Fe/Al_2O_3 coatings.

2. Alumina particles can induce a ceramic property in the coating, and this ceramic state increases the mechanical properties of the coating to the point that the Vickers hardness for the row material was 585 Vickers and for the layer containing 50 g/l of alumina reached about 750 Vickers HV0.05. The main reason is the increase in hardness inside the microstructure where the Al_2O_3 ceramic particles prevent the movement of dislocations and grain boundaries.

3. SEM images correctly showed the locations of Al_2O_3 particles in the coating. These particles are sometimes spherical and very smooth. After mixing with the background (nickel), they slowly turn into relatively soft particles, which change the path and mechanism of grain growth, and in SEM images, more smooth particles are seen.

4. Chemical polarization and Varna quest diagrams showed that the chemical properties of the sample containing Al_2O_3 particles are much better, and this sample is damaged and corroded much later. Corrosion in the coating containing Al_2O_3 is reported to be about ten times less than the raw material. Al_2O_3 hardeners are a ceramic phase; therefore, there is a very high corrosion resistance located on the surface of the coating between the corrosive solution and the layer, which causes corrosion on the metal base at the grain boundary

5. Wear and corrosion tests on the sample containing alumina particles proved that the presence of these particles increases the corrosion resistance to the extent that the coefficient of friction of the sample containing alumina was much higher (0.35) than the raw material (0.21),
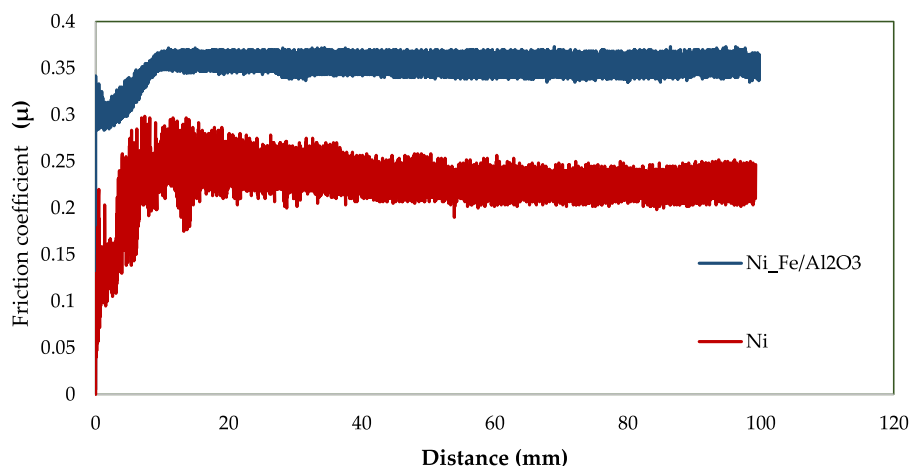
Fig. 8. Friction coefficient changes of Ni and Ni–Fe/Al$_2$O$_3$ coatings.
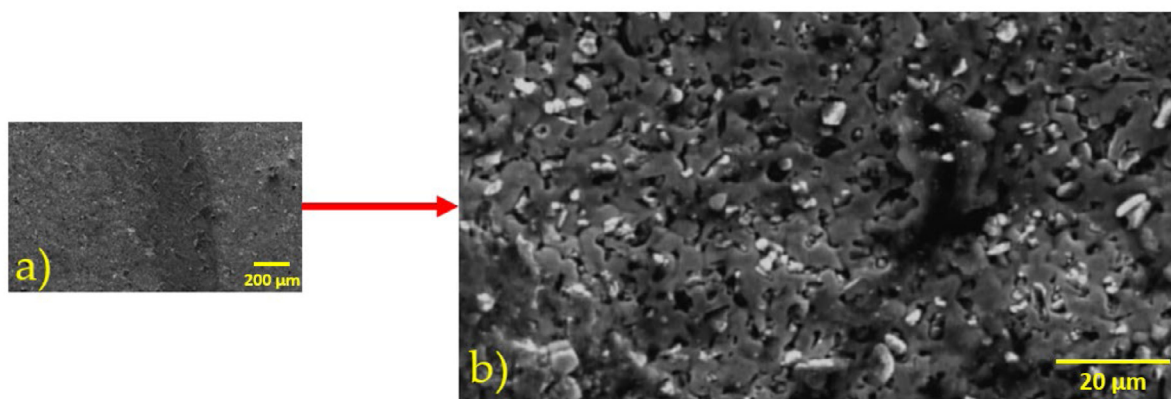

Fig. 9. SEM image of wear bar and surface morphology of the Ni–Fe/Al2O3 composite coating.

which means minor damage to the sample with alumina particles coating. Al$_2$O$_3$ particles and the hardness increase the wear resistance and change the wear mechanism from layered wear to scratch abrasion.

CRediT authorship contribution statement

Mohammad Rezayat: Writing and revising. **Morteza Saghafi Yazdi:** Administrator, Idea. **Mohammad Damous Zandi:** Draw figures and analysis. **Aref Azami:** Writing and revising.

Declaration of competing interest

The authors declare that they have no known competing financial interests or personal relationships that could have appeared to influence the work reported in this paper.

Acknowledgment

References

Al-Faysal, 2018. Decomposition of methane over alumina supported fe and Ni–Fe bimetallic catalyst: Effect of preparation procedure and calcination temperature. J. Saudi Chem. Soc. 22 (2).

Alimadadi, H., Ahmadi, M., Aliofkhazraei, M., Younesi, S.R., 2009. Corrosion properties of electrodeposited nanocrystalline and amorphous patterned Ni–W alloy. Mater. Des. 30 (4), 1356–1361. http://dx.doi.org/10.1016/j.matdes.2008.06.036.

Aliofkhazraei others, M., 2021. Development of electrodeposited multilayer coatings: A review of fabrication, microstructure, properties and applications. Appl. Surf. Sci. Adv. 6, 100141. http://dx.doi.org/10.1016/j.apsadv.2021.100141.

Asa Deepthi others, K., 2016. Physical and electrical characteristics of NiFe thin films using ultrasonic assisted pulse electrodeposition. Appl. Surf. Sci. 360, 519–524.

Ataee-Esfahani, H., Vaezi, M.R., Nikzad, L., Yazdani, B., Sadrnezhaad, S.K., 2009. Influence of SiC nanoparticles and saccharin on the structure and properties of electrodeposited Ni–Fe/SiC nanocomposite coatings. J. Alloys Compd. 484 (1–2), 540–544. http://dx.doi.org/10.1016/j.jallcom.2009.04.146.

Azami, A., Azizi, A., Khoshanjam, A., Hadad, M., 2020. A new approach for nanofinishing complicated surfaces using rotational abrasive finishing process. Mater. Manuf. Process. 35 (8), 940–950. http://dx.doi.org/10.1080/10426914.2020.1750631.

Bonino, J.-P., 1997. Thermal stability of electrodeposited Ni–P alloys. J. Appl. Electrochem. 27 (10), 1193–1197.

Chandrasekar, M.S., Pushpavanam, M., 2008. Pulse and pulse reverse plating—Conceptual, advantages and applications. Electrochim. Acta 53 (8), 3313–3322. http://dx.doi.org/10.1016/j.electacta.2007.11.054.

Chaudhari, A.K., Singh, V.B., 2018. A review of fundamental aspects, characterization and applications of electrodeposited nanocrystalline iron group metals, Ni-Fe alloy and oxide ceramics reinforced nanocomposite coatings. J. Alloys Compd. 751, 194–214. http://dx.doi.org/10.1016/j.jallcom.2018.04.090.

Chintada, V.B., Koona, R., Raju Bahubalendruni, M.V.A., 2021. State of art review on nickel-based electroless coatings and materials. J. Bio- Tribo-Corros. 7 (4), http://dx.doi.org/10.1007/s40735-021-00568-7.

Etminanfar, M.R., Heydarzadeh Sohi, M., 2012. Corrosion resistance of multilayer coatings of nanolayered Cr/Ni electrodeposited from Cr(III)–Ni(II) bath. Thin Solid Films 520 (16), 5322–5327. http://dx.doi.org/10.1016/j.tsf.2012.03.127.

Fiebig others, J., 2016. Deformation behavior of multilayered NiFe with bimodal grain size distribution at room and elevated temperature. Mater. Sci. Eng. A 656, 174–183. http://dx.doi.org/10.1016/j.msea.2015.12.075.

Góral, A., Nowak, M., Berent, K., Kania, B., 2014. Influence of current density on microstructure and properties of electrodeposited nickel-alumina composite coatings. J. Alloys Compd. 615, S406–S410. http://dx.doi.org/10.1016/j.jallcom.2014.01.025.

Gupta, M., Podlaha, E.J., 2010. Electrodeposition of CuNiW alloys: thin films, nanostructured multilayers and nanowires. J. Appl. Electrochem. 40 (7), 1429–1439. http://dx.doi.org/10.1007/s10800-010-0120-z.

Karmakar, R., Maji, P., Ghosh, S.K., 2020. A review on the nickel based metal matrix composite coating. Met. Mater. Int. 27 (7), 2134–2145. http://dx.doi.org/10.1007/s12540-020-00872-w.

Kim, S.H., Baik, Y.J., Kwon, D., 2004. Analysis of interfacial strengthening from composite hardness of TiN/VN and TiN/NbN multilayer hard coatings. Surf. Coat. Technol. 187 (1), 47–53. http://dx.doi.org/10.1016/j.surfcoat.2004.01.011.

Lajevardi, S.A., Shahrabi, T., Szpunar, J.A., 2013. Synthesis of functionally graded nano Al2O3–Ni composite coating by pulse electrodeposition. Appl. Surf. Sci. 279, 180–188. http://dx.doi.org/10.1016/j.apsusc.2013.04.067.

Lumley, R., Morton, A., Polmear, I., 2006. Nanoengineering of metallic materials. Nanostruct. Control Mater. 219–250. http://dx.doi.org/10.1533/9781845691189.219.

Maillé, L., Aubert, P., Sant, C., Garnier, P., 2004. A mechanical study of W–N/W multilayers. Surf. Coat. Technol. 180–181, 483–487. http://dx.doi.org/10.1016/j.surfcoat.2003.10.092.

Majidi, H., Aliofkhazraei, M., 2016. Corrosion and wear behaviour of multilayer pulse electrodeposited Ni–Al2O3 nanocomposite coatings assisted with ultrasound. Bull. Mater. Sci. 39 (7), 1691–1699. http://dx.doi.org/10.1007/s12034-016-1307-7.

Major, L., 2014. Wear mechanisms of multilayer TiN/Ti/a-C:H coatings investigated by transmission electron microscopy technique. Arch. Civ. Mech. Eng. 14 (4), 615–621. http://dx.doi.org/10.1016/j.acme.2014.01.007.

Raghavendra, C.R., Basavarajappa, S., Sogalad, I., 2018. Electrodeposition of Ni-nano composite coatings: a review. Inorg. Nano-Metal Chem. 48 (12), 583–598. http://dx.doi.org/10.1080/24701556.2019.1567537.

Rezayat, M., Yazdi, M., Noghani, M., Ahmadi, R., 2020. Bactericidal properties of copper-tin nanoparticles on escherichia coli in a liquid environment. Plasma 3, 153–165.

Sajjadnejad, M., Mozafari, A., Omidvar, H., Javanbakht, M., 2014. Preparation and corrosion resistance of pulse electrodeposited Zn and Zn–SiC nanocomposite coatings. Appl. Surf. Sci. 300, 1–7. http://dx.doi.org/10.1016/j.apsusc.2013.12.143.

Srivastava, M., William Grips, V.K., Jain, A., Rajam, K.S., 2007. Influence of SiC particle size on the structure and tribological properties of Ni–Co composites. Surf. Coat. Technol. 202 (2), 310–318. http://dx.doi.org/10.1016/j.surfcoat.2007.05.078.

Starosta, R., Zielinski, A., 2004. Effect of chemical composition on corrosion and wear behaviour of the composite Ni–Fe–Al2O3 coatings. J. Mater. Process. Technol. 157–158, 434–441.

Thiemig, D., Bund, A., Talbot, J.B., 2009. Influence of hydrodynamics and pulse plating parameters on the electrocodeposition of nickel–alumina nanocomposite films. Electrochim. Acta 54 (9), 2491–2498. http://dx.doi.org/10.1016/j.electacta.2008.04.004.

Torabinejad, V., 2016. Ni–Fe–Al2O3 electrodeposited nanocomposite coating with functionally graded microstructure. Bull. Mater. Sci. 39 (3), 857–864. http://dx.doi.org/10.1007/s12034-016-1211-1.

Torabinejad, V., Aliofkhazraei, M., Assareh, S., Allahyarzadeh, M.H., Rouhaghdam, A.S., 2017a. Electrodeposition of Ni-Fe alloys, composites, and nano coatings–A review. J. Alloys Compd. 691, 841–859. http://dx.doi.org/10.1016/j.jallcom.2016.08.329.

Torabinejad, V., Aliofkhazraei, M., Rouhaghdam, A.S., Allahyarzadeh, M.H., 2017b. Tribological performance of Ni-Fe-Al2O3 multilayer coatings deposited by pulse electrodeposition. Wear 380–381, 115–125. http://dx.doi.org/10.1016/j.wear.2017.03.013.

Torabinejad, V., Aliofkhazraei, M., Rouhaghdam, A.S., Allahyarzadeh, M.H., 2017c. Tribological properties of Ni-Fe-Co multilayer coatings fabricated by pulse electrodeposition. Tribol. Int. 106, 34–40. http://dx.doi.org/10.1016/j.triboint.2016.10.025.

Torabinejad, V., Aliofkhazraei, M., Rouhaghdam, A.S., Allahyarzadeh, M.H., Kasama, T., Alimadadi, H., 2017d. Mechanical properties of multilayer Ni-Fe and Ni-Fe-Al2O3 nanocomposite coating. Mater. Sci. Eng. A 700, 448–456. http://dx.doi.org/10.1016/j.msea.2017.06.009.

Torabinejad, V., Rouhaghdam, A.S., Aliofkhazraei, M., Allahyarzadeh, M.H., 2016. Electrodeposition of Ni–Fe and Ni–Fe-(nano Al 2 O 3) multilayer coatings. J. Alloys Compd. 657, 526–536. http://dx.doi.org/10.1016/j.jallcom.2015.10.154.

Troyon, M., Wang, L., 1996. Influence of saccharin on the structure and corrosion resistance of electrodeposited multilayers. Appl. Surf. Sci. 103 (4), 517–523. http://dx.doi.org/10.1016/s0169-4332(96)00555-7.

Vitry, V., Kanta, A.-F., Delaunois, F., 2012. Application of nitriding to electroless nickel–boron coatings: Chemical and structural effects; mechanical characterization; corrosion resistance. Mater. Des. 39, 269–278. http://dx.doi.org/10.1016/j.matdes.2012.02.037.

Wasekar, N.P., Sundararajan, G., 2015. Sliding wear behavior of electrodeposited Ni–W alloy and hard chrome coatings. Wear 342–343, 340–348. http://dx.doi.org/10.1016/j.wear.2015.10.003.

Zhang, W., Deng, H., Li, H., Yao, S., Wang, H., 2015. Synthesis and magnetic properties of Ni–Fe/Cu/Co/Cu multilayer nanowire arrays. J. Mater. Sci. Mater. Electron. 26 (4), 2520–2524. http://dx.doi.org/10.1007/s10854-015-2716-x.